Aalborg Universitet

AALBORG UNIVERSITY
DENMARK

A Mode-Adaptive Power-Angle Control Method for Transient Stability Enhancement of Virtual Synchronous Generators

Wu, Heng; Wang, Xiongfei

Published in:
I E E E Journal of Emerging and Selected Topics in Power Electronics

DOI (link to publication from Publisher):
10.1109/JESTPE.2020.2976791

Publication date:
2020

Document Version
Accepted author manuscript, peer reviewed version

Link to publication from Aalborg University

Citation for published version (APA):
Wu, H., & Wang, X. (2020). A Mode-Adaptive Power-Angle Control Method for Transient Stability Enhancement of Virtual Synchronous Generators. *I E E E Journal of Emerging and Selected Topics in Power Electronics*, *8*(2), 1034-1049. [9016216]. https://doi.org/10.1109/JESTPE.2020.2976791

General rights
Copyright and moral rights for the publications made accessible in the public portal are retained by the authors and/or other copyright owners and it is a condition of accessing publications that users recognise and abide by the legal requirements associated with these rights.

- Users may download and print one copy of any publication from the public portal for the purpose of private study or research.
- You may not further distribute the material or use it for any profit-making activity or commercial gain
- You may freely distribute the URL identifying the publication in the public portal -

Take down policy
If you believe that this document breaches copyright please contact us at vbn@aub.aau.dk providing details, and we will remove access to the work immediately and investigate your claim.

This article has been accepted for publication in a future issue of this journal, but has not been fully edited. Content may change prior to final publication. Citation information: DOI 10.1109/JESTPE.2020.2976791, IEEE Journal of Emerging and Selected Topics in Power Electronics

A Mode-Adaptive Power-Angle Control Method for Transient Stability Enhancement of Virtual Synchronous Generators

Heng Wu, *Student Member*, *IEEE*, and Xiongfei Wang, *Senior Member*, *IEEE*

***Abstract*—The virtual synchronous generator (VSG) is emerging as an attractive solution for interconnecting converter-based resources with the power grid. However, due to the nonlinear power-angle relationship, VSGs are, similarly to synchronous generators, prone to the loss of synchronization (LOS) under large grid disturbances. This paper thus analyzes the large-signal synchronization stability, i.e., the transient stability of grid-connected VSGs, and then proposes a mode-adaptive power-angle control method for enhancing the transient stability. In this approach, the positive-feedback mode of the power-angle control of the VSG is detected and adaptively switched to the negative-feedback mode after large disturbances. Thus, the LOS of the VSG can be avoided when there are equilibrium points after the disturbance. Moreover, during severe grid faults without any equilibrium points, a bounded dynamic response of the power angle can be obtained with the mode-adaptive control, and the VSG can still be stabilized even if the fault clearing time is beyond the critical clearing time. These superior features prevent the VSG-based system from collapsing due to the delayed fault clearance or the malfunction of protective relays. Finally, time-domain simulations and experimental tests are performed to verify the effectiveness of the control method.**

***Index Terms*— Transient stability, virtual synchronous generator, power control.**

I. INTRODUCTION

Power-electronic-based power systems are being envisioned in the near future, owing to the widespread use of power electronic converters in renewable energy resources, energy-efficient power loads, and flexible power transmission and distribution systems. Unlike synchronous generators (SGs), the dynamics of power converters are highly dependent on their digital control algorithms, which feature multiple-timescale, programmable and highly nonlinear [1]. Thus, there have been continuous research efforts on developing control methods for grid-connected converters in order to improve the interoperability and stability of converter-based power systems [2].

The virtual synchronous generator (VSG) control, among other alternative control schemes, is emerging as an attractive approach for reliably operating converter-based power systems [3]-[4]. A prominent feature of the VSG control scheme lies in emulating the power-angle dynamic of SGs, and thus converters can actively reduce the rate of change of frequency (RoCoF) and the frequency nadir of the system [5]. Moreover, by using the power-angle control, the small-signal synchronization stability of converters under low short-circuit ratio (SCR) grid conditions can be significantly enhanced [6].

A number of research works have been reported on the modeling and dynamic analysis of VSGs under different grid conditions [7]-[9]. Yet, most of them are focused on the small-signal stability, where the findings cannot be readily extended to characterize the large-signal nonlinear dynamics of VSGs. A few research works are available on analyzing the large-signal synchronization stability, i.e., the *transient stability*, of VSGs [10]. When the solid fault occurs near the point of common coupling (PCC), the VSG is generally switched to the vector current control for limiting the current, where the grid synchronization is realized by the backup phase-locked loop (PLL) [6], [11]-[12]. The transient stability impacts of the current limit control and the PLL have been discussed in [13]-[18]. In contrast, for the large disturbances that do not provoke the current limit control of the VSG, e.g., the switching of transmission lines, the high-impedance fault [19], or the remote fault [20], the VSG will retain its power-angle control during the disturbances, and tends to have the similar transient stability challenges as SGs, i.e., the power imbalance caused by the large disturbance may drive VSGs to cross over the unstable equilibrium point (UEP) along the power-angle curve, leading to a positive feedback power-angle control and the consequent loss of synchronization (LOS) [21].

Conventionally, in order to improve the transient stability of the SG-based power system, the high-speed protective relays and circuit breakers are utilized to clear the fault in time [21]-[22]. Yet, this method cannot handle the transient instability resulted from the disturbances which are not related to grid faults [21]. Moreover, the possible malfunction of relays and circuit breakers may further jeopardize the transient stability or even lead to the power system collapse [22]. Hence, instead of solely relying on the protection devices, it is worth exploring the control methods of VSGs under large disturbances. In [10],

This work was supported by the Aalborg University Strategic Talent Management Programme. (*Corresponding author: Xiongfei Wang.*)

H. Wu and X. Wang are with the Department of Energy Technology, Aalborg University, 9220 Aalborg, Denmark (e-mail: hew@et.aau.dk; xwa@et.aau.dk).

2168-6777 (c) 2019 IEEE. Personal use is permitted, but republication/redistribution requires IEEE permission. See http://www.ieee.org/publications_standards/publications/rights/index.html for more information.
Authorized licensed use limited to: Aalborg Universitetsbibliotek. Downloaded on March 09,2020 at 13:04:12 UTC from IEEE Xplore. Restrictions apply.

This article has been accepted for publication in a future issue of this journal, but has not been fully edited. Content may change prior to final publication. Citation information: DOI 10.1109/JESTPE.2020.2976791, IEEE Journal of Emerging and Selected Topics in Power Electronics

the transient stability enhancement methods of SGs, which include controlling the governor to reduce the accelerating power and utilizing fast excitation control to increase the restoring synchronization power [21]-[22], have been introduced for VSGs. Alternatively, inspired by the full controllability of VSGs, the methods of adaptively changing the inertia and damping ratio of VSGs during large disturbances are also reported to dampen the power and frequency oscillations [23]-[26]. All those control schemes do, to some extent, mitigate, but cannot fully eliminate, the risk of VSGs from crossing over the UEP along the power-angle curve after the disturbance [10]. Moreover, the positive feedback mode of the power-angle control after the UEP is still unchanged. Consequently, the risk of LOS persists whenever the VSG crosses over the UEP after the disturbance [10].

In our previous work [11], it is demonstrated that if the converter is merely controlled with the power-frequency droop, e.g., power synchronization control [6], its active power loop emerges as the first-order control loop, and the risk of crossing over the UEP after the disturbance can be avoided. While the first-order active power loop brings in better transient stability performance, the lack of inertia contribution from the converter might threat the frequency stability of the power system. Therefore, the transient stability enhancement method of the converter with the VSG control is still demanded.

This paper thus proposes a mode-adaptive power angle control method for enhancing the transient stability of VSGs. The basic idea of this approach is to detect the feedback mode of the power-angle control loop after a large disturbance, and then adaptively switch the loop gain from the positive-feedback to the negative-feedback mode. Thus, the positive-feedback operation of the power- angle control of the VSG can be prevented, and the risk of LOS can then be eliminated when the system has equilibrium points after the disturbance. Moreover, in the absence of equilibrium points during severe grid faults, a bounded dynamic response of the power angle can be obtained with the mode-adaptive control, and the VSG can be stabilized even if the fault clearing time (FCT) is beyond the critical clearing time (CCT). The rigorous mathematical proof for the transient stability enhancement of the mode-adaptive power-angle control is presented. Time-domain simulations and experimental results corroborate the effectiveness of the theoretical analysis and the control approach.

II. Transient Stability Basics of VSG-Based Power Systems

A. Dynamic Representation of VSGs for Transient Stability Study

Fig. 1 shows a general system diagram of the grid-connected VSG. The VSG is connected to the grid through a transformer and two paralleled transmission lines. X_T, Z_{g1}~Z_{g3} represent the transformer's leakage reactance and transmission line impedances, respectively. S1~S4 are circuit breakers, and Z_{gnd} denotes the grounding impedance when the symmetrical three-phase to ground fault occurs. Since the main concern of this work is the transient stability impact of the power-angle control of the VSG, the power grid is modeled as an equivalent impedance (R_g+jX_g) in series with infinite bus voltage v_g. i_g is the current of the VSG injected to the grid, and X_f represents the output filter reactance of the VSG.

An inner voltage loop is used to regulate the PCC voltage v_{PCC} to track its reference v_{PCCref}, where the overcurrent limit is embedded. V_{mref} and θ_{ref} denote the magnitude and the phase angle of v_{PCCref}, respectively. In practice, to actively support the system frequency, the energy storage unit is usually added into the renewable energy sources of the VSG, where the dc-link voltage of the VSG is controlled by the energy storage converter to balance the intermittent power of renewable energy sources and the power demanded from the grid [5]. Hence, the DC-link voltage can be assumed constant when analyzing the interaction between the grid-connected VSG and the power grid [10]-[13].

In the VSG control scheme, the phase reference θ_{ref} is generated from the active power control loop, which is implemented to mimic the second-order swing equation of the SG [21]:

$$P_{ref} - P_e - D\dot{\delta} = 2H\ddot{\delta}. \tag{1}$$

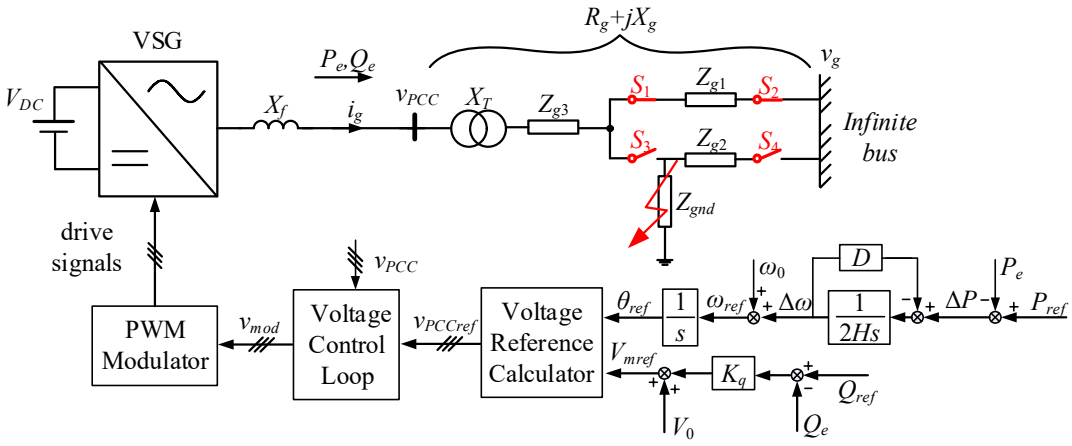

Fig. 1. General system diagram of a grid-connected VSG.

2168-6777 (c) 2019 IEEE. Personal use is permitted, but republication/redistribution requires IEEE permission. See http://www.ieee.org/publications_standards/publications/rights/index.html for more information.
Authorized licensed use limited to: Aalborg Universitetsbibliotek. Downloaded on March 09,2020 at 13:04:12 UTC from IEEE Xplore. Restrictions apply.

This article has been accepted for publication in a future issue of this journal, but has not been fully edited. Content may change prior to final publication. Citation information: DOI 10.1109/JESTPE.2020.2976791, IEEE Journal of Emerging and Selected Topics in Power Electronics

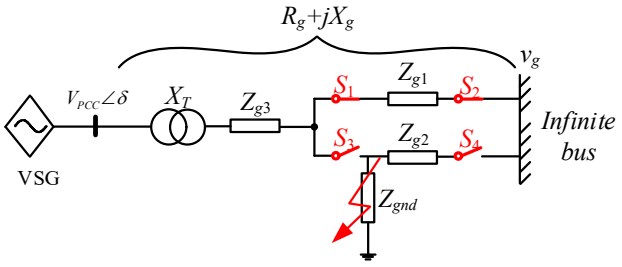

Fig. 2. Equivalent circuit of the VSG used for the transient stability study.

where H is the inertia constant, D is the damping coefficient, and δ is the power angle, which is defined as the phase difference between v_{PCC} and v_g, i.e., $\delta = \theta_{PCC} - \theta_g$ [21]. P_{ref} and P_e are the active power reference and the output active power of the VSG, respectively. The voltage magnitude reference V_{mref} is determined by the reactive power control loop, where the reactive power-voltage (Q-V) droop control is adopted [27], which is given by

$$V_{mref} = V_0 + K_q\left(Q_{ref} - Q_e\right). \tag{2}$$

where V_0 is the nominal voltage magnitude. Q_{ref} and Q_e are the reactive power reference and the output reactive power of the VSG, respectively. K_q is the Q-V droop coefficient.

It is worth noting that the outer power control loops are generally designed with a much lower bandwidth than that of the inner voltage control loop [28]. The transient stability of the VSG is mainly determined by the outer power control loops, and the inner voltage loop can be assumed as a unity gain with an ideal voltage reference tracking during the transient stability analysis, i.e., v_{PCC}=v_{PCCref}. This assumption has been justified in recent studies on the transient stability of grid-connected converters [11]-[18], and will be further proved by the simulations and experimental tests in this work.

Fig. 2 illustrates the equivalent circuit of the grid-connected VSG, where the VSG is simplified as a controlled voltage source. The output active power and reactive power of the VSG can be expressed as [27]:

$$P_e = \frac{3}{2}\left[\alpha\left(V_{PCC}^2 - V_{PCC}V_g\cos\delta\right) + \beta V_{PCC}V_g\sin\delta\right]. \tag{3}$$

$$Q_e = \frac{3}{2}\left[\beta\left(V_{PCC}^2 - V_{PCC}V_g\cos\delta\right) - \alpha V_{PCC}V_g\sin\delta\right]. \tag{4}$$

where α and β are given by

$$\alpha = \frac{R_g}{R_g^2 + X_g^2} \tag{5}$$

$$\beta = \frac{X_g}{R_g^2 + X_g^2}. \tag{6}$$

Substituting (4) into (2) together with V_{PCC}=V_{mref}, the relationship between V_{PCC} and δ can be revealed, which is given as (7) at the end of this page.

Substituting (7) into (3), the P_e-δ curves with different Q-V droop coefficients and different R_g/X_g ratios can be plotted, as shown in Fig. 3. It can be seen that the power transfer capability of the VSG varies with different Q-V droop coefficients and R_g/X_g ratios [10]. Nevertheless, all P_e-δ curves have the same trend that P_e is first monotonously increased to its peak value with the increasing of δ, and then monotonously decreased to zero. Such a nonlinear P_e-δ relationship is the root cause of the transient instability of the VSG (SG) [21].

B. Types of Transient Stability Problems

Fig. 4 illustrates the conceptual P_e-δ curves of the VSG before and after the disturbance, respectively. Only the large disturbances that do not provoke the overcurrent limit of the VSG, i.e., the switching of transmission lines and the high impedance fault, are of concern in this work. The transient stability of the VSG when it switches to the current limit control has been extensively discussed in [13]-[18], and thus, will not be repeated.

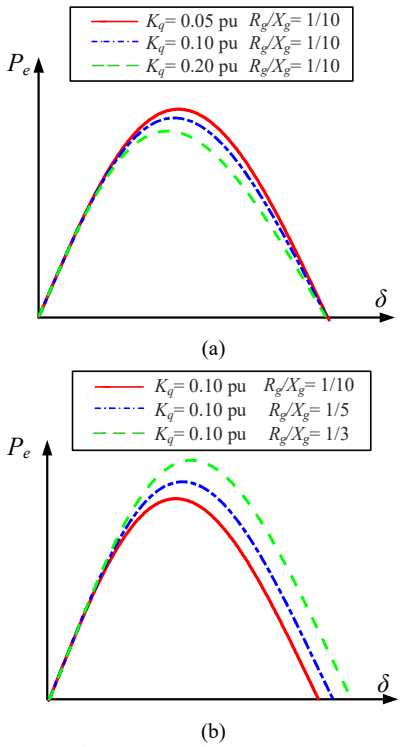

Fig. 3. P_e-δ curves with different Q-V droop coefficients and different R_g/X_g ratios. (a) Different Q-V droop coefficients. (b) Different R_g/X_g ratios.

$$V_{PCC} = \frac{1.5K_q\beta V_g\cos\delta + 1.5K_q\alpha V_g\sin\delta - 1 + \sqrt{\left(1.5K_q\beta V_g\cos\delta + 1.5K_q\alpha V_g\sin\delta - 1\right)^2 + 6K_q\beta\left(V_0 + K_qQ_{ref}\right)}}{3K_q\beta}. \tag{7}$$

2168-6777 (c) 2019 IEEE. Personal use is permitted, but republication/redistribution requires IEEE permission. See http://www.ieee.org/publications_standards/publications/rights/index.html for more information.
Authorized licensed use limited to: Aalborg Universitetsbibliotek. Downloaded on March 09,2020 at 13:04:12 UTC from IEEE Xplore. Restrictions apply.

This article has been accepted for publication in a future issue of this journal, but has not been fully edited. Content may change prior to final publication. Citation information: DOI 10.1109/JESTPE.2020.2976791, IEEE Journal of Emerging and Selected Topics in Power Electronics

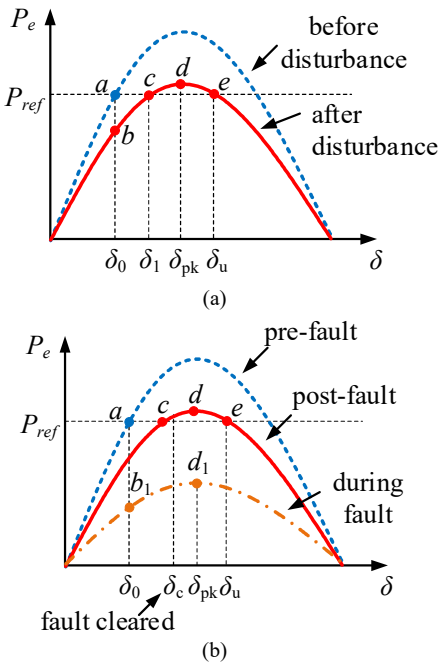

Fig. 4. P_e-δ curves. (a) With equilibrium points after a transient disturbance, dashed line: before disturbance, solid line: after disturbance. (b) Without equilibrium points during a grid fault, dashed line: pre-fault, dashed dotted line: during fault, solid line: post-fault. [21]

As shown by dashed lines in Fig. 4, the two transmission lines are initially in service and the VSG operates at the equilibrium point a, where $P_{ref} = P_e$ in the steady state. There are basically two types of transient stability problems, depending on whether the system has equilibrium points after a disturbance, which are illustrated as follows [21]:

1) Type-I: Presence of Equilibrium Points

Fig. 4(a) shows the P_e-δ curves for the type-I transient stability problem, where equilibrium points exist after a disturbance. As illustrated by the solid line in Fig. 4(a), the points c and e represent the stable equilibrium point (SEP) and the UEP after the disturbance, respectively [21]. According to the swing equation given by (1), the output frequency of the VSG increases from the point b to the point c due to $P_{ref} > P_e$, and then decreases from the point c to the UEP e due to $P_{ref} < P_e$. If the output frequency of the VSG fails to recover to the grid frequency before the UEP e. The VSG will crossover the UEP e and its output frequency turns to increase again due to $P_{ref} > P_e$, which leads to the LOS of the system.

2) Type-II: No Equilibrium Points

Fig. 4(b) shows the P_e-δ curves for the type-II transient stability problem, where no equilibrium points exist after the fault. The P_e-δ curves during the fault and after the fault clearance are illustrated by the dashed-dotted and solid lines in Fig. 4(b), respectively. The output frequency of the VSG keeps increasing during the fault due to $P_{ref} > P_e$ and can only be decreased after the fault clearance. Since the transient stability of the system requires the VSG not to crossover the UEP e, the fast fault clearance is of importance. The largest fault clearing angle and time which prevent the transient instability of the system are known as the critical clearing angle (CCA) and CCT [21].

III. Mode-Adaptive Power-Angle Control of VSGs

A. Basic Idea

Fig. 5 illustrates the equivalent control diagram of the active power loop of the VSG, which is derived from Fig. 1, eq. (3) and (7). For the Type-I transient stability problem with equilibrium points, the active power control enlarges the control error ΔP, rather than reducing it whenever δ is beyond δ_u (the corresponding power angle of the UEP e) shown in Fig. 4(a), which leads to a positive-feedback power-angle control and thus the instability is inevitable. Similarly, for the type-II transient stability problem without any equilibrium points, the positive-feedback power-angle control can also be observed whenever δ is beyond δ_{pk} shown in Fig. 4(b). Hence, there are two feedback modes of the power-angle control of the VSG, i.e., the negative-feedback mode and the positive-feedback mode, which are depicted in Fig. 6.

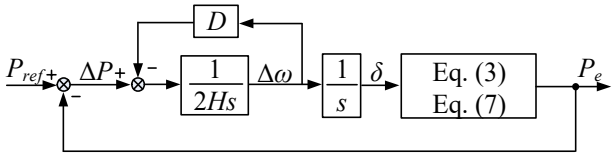

Fig. 5. Control diagram of the active power loop of the VSG.

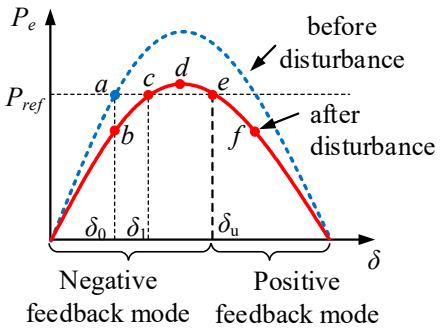

Fig. 6. The negative-feedback mode and the positive-feedback mode of the power angle control of the VSG. (a) With equilibrium points. (b) Without equilibrium points.

2168-6777 (c) 2019 IEEE. Personal use is permitted, but republication/redistribution requires IEEE permission. See http://www.ieee.org/publications_standards/publications/rights/index.html for more information.
Authorized licensed use limited to: Aalborg Universitetsbibliotek. Downloaded on March 09,2020 at 13:04:12 UTC from IEEE Xplore. Restrictions apply.

This article has been accepted for publication in a future issue of this journal, but has not been fully edited. Content may change prior to final publication. Citation information: DOI 10.1109/JESTPE.2020.2976791, IEEE Journal of Emerging and Selected Topics in Power Electronics

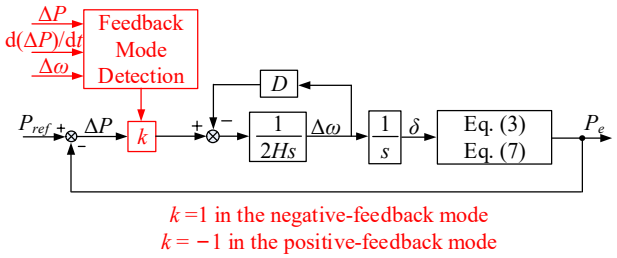

Fig. 7. Block diagram of the active power loop of the VSG with the mode-adaptive control.

In order to avoid the positive-feedback mode of the power-angle control, a mode-adaptive power angle control of the VSG is proposed in this work. The general idea of the method is illustrated in Fig. 7, where a control variable k is inserted in the forward path of the active power loop, which is set as a positive unity gain (i.e. 1) in the negative-feedback mode, and is switched to the negative unity gain (i.e. −1) in the positive-feedback mode. Thus, the power-angle control loop can be kept as a negative-feedback loop, and the transient stability of the VSG can be guaranteed as long as there are equilibrium points after a disturbance. Therefore, the Type-I transient stability problem described in Section II-B can be avoided.

For the Type-II transient stability problem without any equilibrium points, the mode-adaptive control limits the oscillation of the power angle δ around δ_{pk} with a bounded dynamic, which is elaborated by the arrows in Fig. 6(b). This is a superior feature over the conventional SGs, whose power angle δ will diverge if there are no equilibrium points. Moreover, as long as the equilibrium points are restored by the fault clearance (even if FCT > CCT), it turns to the Type-I transient stability problem, and the VSG system can always be stabilized by the mode-adaptive control.

B. Detection of the Feedback Mode

From Fig. 7, it is clear that the feedback mode detection plays a critical role in the mode-adaptive power-angle control. Considering the Type-I and Type-II transient stability problems, the principles of the feedback-mode detection are elaborated as follows:

For the Type-I transient stability problem, three possible operating scenarios of the VSG can be observed from Fig. 6(a), depending on whether the VSG will cross the point d and e during a disturbance, i.e.

i) No crossing of the point d, stable (negative-feedback mode).

ii) Crossing the point d but not crossing the UEP e, stable (negative-feedback mode).

iii) Crossing the UEP e, unstable (positive-feedback mode).

Accordingly, the operating regions for these three scenarios can be defined, which are summarized in Table I-III. The operating characteristic of the VSG in the specific region can be characterized by the signs of the state variables ΔP, $\mathrm{d}(\Delta P)/\mathrm{d}t$ and $\Delta\omega$, which are also listed in Tables I-III. For example, in the region $b\rightarrow c$, it is known from Fig. 6(a) that $P_{ref} > P_e$ ($\Delta P > 0$), and then the active power loop (see Fig. 5) increases the output frequency of the VSG to reduce the control error ΔP, which leads to $\Delta\omega > 0$ and $\mathrm{d}(\Delta P)/\mathrm{d}t < 0$.

For the Type-II transient stability problem, due to the absence of equilibrium points, $P_{ref} > P_e$ always holds, and the crossing of the point d_1 is inevitable, as shown in Fig. 6(b). The corresponding operation regions and the status of state variables in this scenario are summarized in Table IV.

TABLE I (TYPE I TRANSIENT STABILITY PROBLEM)
STABLE OPERATION OF THE VSG, NO CROSSING OF THE POINT D

Operation region	Feedback mode	ΔP	$\mathrm{d}(\Delta P)/\mathrm{d}t$	$\Delta\omega$
$b\rightarrow c$	negative	>0	<0	>0
$c\rightarrow d$	negative	<0	<0	>0
$d\rightarrow c$	negative	<0	>0	<0
$c\rightarrow b$	negative	>0	>0	<0

TABLE II (TYPE I TRANSIENT STABILITY PROBLEM)
STABLE OPERATION OF THE VSG, CROSSING THE POINT D BUT NOT CROSSING THE POINT E

Operation region	Feedback mode	ΔP	$\mathrm{d}(\Delta P)/\mathrm{d}t$	$\Delta\omega$
$b\rightarrow c$	negative	>0	<0	>0
$c\rightarrow d$	negative	<0	<0	>0
$d\rightarrow e$	negative	<0	>0	>0
$e\rightarrow d$	negative	<0	<0	<0
$d\rightarrow c$	negative	<0	>0	<0
$c\rightarrow b$	negative	>0	>0	<0

2168-6777 (c) 2019 IEEE. Personal use is permitted, but republication/redistribution requires IEEE permission. See http://www.ieee.org/publications_standards/publications/rights/index.html for more information.
Authorized licensed use limited to: Aalborg Universitetsbibliotek. Downloaded on March 09,2020 at 13:04:12 UTC from IEEE Xplore. Restrictions apply.

This article has been accepted for publication in a future issue of this journal, but has not been fully edited. Content may change prior to final publication. Citation information: DOI 10.1109/JESTPE.2020.2976791, IEEE Journal of Emerging and Selected Topics in Power Electronics

TABLE III (TYPE I TRANSIENT STABILITY PROBLEM)
UNSTABLE OPERATION OF THE VSG, CROSSING THE POINT E

Operation region	Feedback mode	ΔP	$\mathrm{d}(\Delta P)/\mathrm{d}t$	$\Delta\omega$
$b \rightarrow c$	negative	>0	<0	>0
$c \rightarrow d$	negative	<0	<0	>0
$d \rightarrow e$	negative	<0	>0	>0
Cross e	**positive**	**>0**	**>0**	**>0**

TABLE IV (TYPE-II TRANSIENT STABILITY PROBLEM)
UNSTABLE OPERATION OF THE VSG, CROSSING THE POINT D1

Operation region	Feedback mode	ΔP	$\mathrm{d}(\Delta P)/\mathrm{d}t$	$\Delta\omega$
$b_1 \rightarrow d_1$	negative	>0	<0	>0
Cross d_1	**positive**	**>0**	**>0**	**>0**

TABLE V (TYPE I TRANSIENT STABILITY PROBLEM)
OPERATING CHARACTERISTIC OF THE VSG BEFORE AND AFTER MOVING BACKWARDS AND CROSSING THE POINT E

Operation region	The value of k	ΔP	$\mathrm{d}(\Delta P)/\mathrm{d}t$	$\Delta\omega$
$e \rightarrow f$	−1	>0	>0	>0
$f \rightarrow e$ (move backwards)	−1	**>0**	<0	<0
Cross e	1	**<0**	<0	<0

TABLE VI (TYPE II TRANSIENT STABILITY PROBLEM)
OPERATING CHARACTERISTIC OF THE VSG BEFORE AND AFTER MOVING BACKWARDS AND CROSSING THE POINT D1

Operation region	The value of k	ΔP	$\mathrm{d}(\Delta P)/\mathrm{d}t$	$\Delta\omega$
$d_1 \rightarrow f_1$	−1	>0	>0	>0
$f_1 \rightarrow d_1$ (move backwards)	−1	>0	**<0**	<0
Cross d_1	1	>0	**>0**	<0

Based on Tables I-IV, it is clear that $\Delta P>0$, $\mathrm{d}(\Delta P)/\mathrm{d}t>0$ and $\Delta\omega>0$ only occur when the VSG operates in the positive-feedback mode, i.e., when crossing the UEP e for the Type-I transient stability problem or crossing the point d_1 for the Type-II transient stability problem, which are highlighted as the last rows of Table III and Table IV. Therefore, $\Delta P>0$, $\mathrm{d}(\Delta P)/\mathrm{d}t>0$ and $\Delta\omega>0$ can be used as a criterion for switching k to −1. Thus, $\Delta\omega$ is decreased, rather than being increased after the UEP e (the point d_1), which finally leads to a decrease of δ. Consequently, the VSG moves backwards along the P_e-δ curve and crosses the UEP e (the point d_1), after which the VSG enters into the negative-feedback mode again and k is switched back to 1 accordingly.

Based on Fig. 6, the operating characteristics of the VSG before and after moving backwards and crossing the UEP e (the point d_1) can be summarized, which are given by Table V and VI. It is noted that ΔP ($\mathrm{d}(\Delta P)/\mathrm{d}t$) changes from the positive (negative) to the negative (positive) value when the VSG moves backwards and crosses the UEP e (the point d_1), as shown in the last two rows of Table V and VI. Moreover, $\Delta\omega<0$ always holds during the backward crossing of the UEP e (the point d_1). Therefore, the criterion for switching k from −1 back to 1 can be summarized as ($\Delta P<0$ or $\mathrm{d}(\Delta P)/\mathrm{d}t>0$) and ($\Delta\omega<0$).

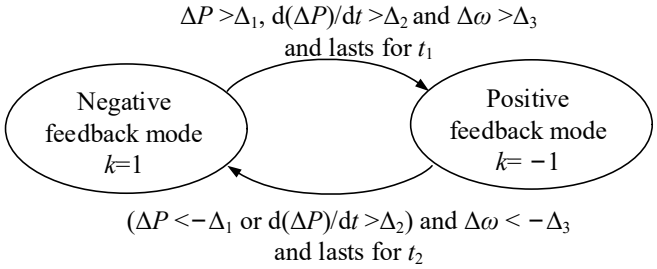

Fig. 8. Overall gain switching logic for the active power loop of the VSG for the Type-I and Type-II transient stability problem.

Fig. 8 illustrates the overall gain switching logic for the VSG. Due to the presence of noises in practice, ΔP, $\mathrm{d}(\Delta P)/\mathrm{d}t$ and $\Delta\omega$ are compared with small positive threshold values (Δ_1, Δ_2, and Δ_3) instead of zero, and the switching criteria should also be met for a given amount of time (t_1 and t_2) before the actual switching of k takes into effect. The larger threshold values lead to a better noise immunity of the gain switching algorithm, but also degrade its sensitivity. A compromise is thus needed in the real application. In this paper, $\Delta_1=1\cdot10^{-5}P_{ref}$, $\Delta_2=1\cdot10^{-3}P_{ref}/s$, $\Delta_3=0.1$ Hz and $t_1=t_2=5$ ms are adopted in both simulations and experimental tests.

2168-6777 (c) 2019 IEEE. Personal use is permitted, but republication/redistribution requires IEEE permission. See http://www.ieee.org/publications_standards/publications/rights/index.html for more information.
Authorized licensed use limited to: Aalborg Universitetsbibliotek. Downloaded on March 09,2020 at 13:04:12 UTC from IEEE Xplore. Restrictions apply.

This article has been accepted for publication in a future issue of this journal, but has not been fully edited. Content may change prior to final publication. Citation information: DOI 10.1109/JESTPE.2020.2976791, IEEE Journal of Emerging and Selected Topics in Power Electronics

Based on Figs. 7 and 8, the proposed mode-adaptive control can be mathematically expressed as:

$$P_{ref}-P_e-D\dot{\delta}=2H\ddot{\delta}\overset{1}{\underset{2}{\rightleftharpoons}}P_e-P_{ref}-D\dot{\delta}=2H\ddot{\delta}$$

$$\begin{aligned}&1.\ \text{if}\ \left\{\left(\Delta P>\Delta_1\right)\&\left(d\left(\Delta P\right)/dt>\Delta_2\right)\&\left(\Delta\omega>\Delta_3\right)\right\}\\&\text{lasts for}\ t_1\\&2.\ \text{if}\ \left\{\left[\left(\Delta P<-\Delta_1\right)|\left(d\left(\Delta P\right)/dt>\Delta_2\right)\right]\&\left(\Delta\omega<-\Delta_3\right)\right\}\\&\text{lasts for}\ t_2\end{aligned}\qquad(8)$$

.

Moreover, it is noted that the measurement and control delays of the VSG is inevitable in practice. Yet, the total delay time is usually around hundreds of microseconds [2], which is much less than the response time of power loops (usually longer than 100 ms [28]) that determine the transient stability of the VSG. Thus, the measurement and control delays of the VSG has negligible impact on the effectiveness of the proposed method. This statement will be further justified by experimental results given in this paper.

It is worth noting that this gain switching logic is generally applicable for all operating scenarios of the VSG, and thus there is no need for the prior knowledge on the type of the transient stability problem. In addition, the proposed method has no specific requirement on the VSG control scheme, which can be readily adapted to other modified/improved VSG control methods.

C. Stability Proof

In this part, the mathematical proof is given to elaborate that the mode-adaptive control can guarantee the transient stability of the VSG as long as the SEP exists after the disturbance. According to Figs. 6(a) and 7, (8) can be equivalently expressed as follows when the SEP exists:

$$\begin{aligned}&P_{ref}-P_e-D\dot{\delta}=2H\ddot{\delta}&&\text{if}\ \delta<\delta_u\\&P_e-P_{ref}-D\dot{\delta}=2H\ddot{\delta}&&\text{if}\ \delta\ge\delta_u\end{aligned}.\qquad(9)$$

As the damping term of the VSG always helps to stabilize the system [21], the worst case assuming a zero damping, i.e., D = 0 is considered here. Consequently, (9) can be simplified as

$$\begin{aligned}&P_{ref}-P_e=2H\ddot{\delta}&&\text{if}\ \delta<\delta_u\\&P_e-P_{ref}=2H\ddot{\delta}&&\text{if}\ \delta\ge\delta_u\end{aligned}.\qquad(10)$$

which is asymptotically stable if its SEP exits, i.e. [29]

1.1) The SEP is Lyapunov stable.

1.2) After the disturbances, the states of the system need to converge to the SEP as $t\to\infty$.

Proof: 1.1) has been proved in [21], and thus only the proof of 1.2) is given as follows:

Without loss of generality, the power angles of SEPs before and after the disturbance are defined as δ_0 and δ_1 in Fig. 9, respectively. After the transient disturbances, it is known from Fig. 9 that the output frequency of the VSG will first increase in the acceleration area where $\delta_0<\delta<\delta_1$, and then decrease in the deceleration area where $\delta_1<\delta<\delta_2$. The VSG can be kept synchronized with the grid if and only if its output frequency is able to recover to the grid frequency [$(d\delta/dt)$=0] in the deceleration area, otherwise its output frequency is always higher than the grid frequency, which inevitably leads to the LOS [21]. Therefore, the sufficient and necessary condition of 1.2) is given as:

1.3) There exists δ_m such that $\delta_1\le\delta_m\le\delta_2$ and $(d\delta_m/dt)=0$, where δ_m is defined as the maximum power angle during the transient [21].

Then, following the same procedure of proving the equal area criterion (EAC) [21], the proof of 1.3) is detailed as follows:

Multiplying both sides of (10) by $2d\delta/dt$, which yields

$$\begin{aligned}&\frac{d\delta}{dt}\cdot\frac{P_{ref}-P_e}{H}=2\frac{d\delta}{dt}\cdot\frac{d^2\delta}{dt^2}=\frac{d}{dt}\left(\frac{d\delta}{dt}\right)^2&&\text{if}\ \delta<\delta_u\\&\frac{d\delta}{dt}\cdot\frac{P_e-P_{ref}}{H}=2\frac{d\delta}{dt}\cdot\frac{d^2\delta}{dt^2}=\frac{d}{dt}\left(\frac{d\delta}{dt}\right)^2&&\text{if}\ \delta\ge\delta_u\end{aligned}.\qquad(11)$$

Integrating both sides of (11) from δ_0 to δ_m, which leads to

$$\int_{\delta_0}^{\delta_m}\frac{\left(P_{ref}-P_e\right)}{H}d\delta=\left(\frac{d\delta_m}{dt}\right)^2-\left(\frac{d\delta_0}{dt}\right)^2\quad.\qquad(12.1)$$
$$\text{if}\ \delta_1\le\delta_m<\delta_u$$

$$\begin{aligned}&\int_{\delta_0}^{\delta_u}\frac{\left(P_{ref}-P_e\right)}{H}d\delta+\int_{\delta_u}^{\delta_m}\frac{\left(P_e-P_{ref}\right)}{H}d\delta\\&=\int_{\delta_0}^{\delta_u}\frac{\left(P_{ref}-P_e\right)}{H}d\delta-\int_{\delta_u}^{\delta_m}\frac{\left(P_{ref}-P_e\right)}{H}d\delta\\&=\left(\frac{d\delta_m}{dt}\right)^2-\left(\frac{d\delta_0}{dt}\right)^2\end{aligned}\quad.\qquad(12.2)$$
$$\text{if}\ \delta_u\le\delta_m\le\delta_2$$

where $(d\delta_0/dt)$ represents the initial frequency deviation of the VSG in respect to the grid frequency, which is zero [21]. Substituting $(d\delta_0/dt)$= 0 into (12), which yields

$$\begin{aligned}&\frac{1}{H}\int_{\delta_0}^{\delta_m}\left(P_{ref}-P_e\right)d\delta=\left(\frac{d\delta_m}{dt}\right)^2\Leftrightarrow\\&\int_{\delta_0}^{\delta_1}\left(P_{ref}-P_e\right)d\delta-\int_{\delta_1}^{\delta_m}\left(P_e-P_{ref}\right)d\delta\\&=H\left(\frac{d\delta_m}{dt}\right)^2\end{aligned}\quad.\qquad(13.1)$$
$$\text{if}\ \delta_1\le\delta_m<\delta_u$$

$$\begin{aligned}&\frac{1}{H}\left[\int_{\delta_0}^{\delta_u}\left(P_{ref}-P_e\right)d\delta-\int_{\delta_u}^{\delta_m}\left(P_{ref}-P_e\right)d\delta\right]=\left(\frac{d\delta_m}{dt}\right)^2\\&\Leftrightarrow\int_{\delta_0}^{\delta_1}\left(P_{ref}-P_e\right)d\delta-\int_{\delta_1}^{\delta_u}\left(P_e-P_{ref}\right)d\delta\\&-\int_{\delta_u}^{\delta_m}\left(P_{ref}-P_e\right)d\delta=H\left(\frac{d\delta_m}{dt}\right)^2\end{aligned}\qquad(13.2)$$
$$\text{if}\ \delta_u\le\delta_m\le\delta_2$$

.

Therefore, 1.3) can be proved if there always exits δ_m which leads to (13.1) =0 or (13.2) =0.

It is known from Fig. 9(b) that the left-hand side of (13.2) can be graphically represented by the area between P_{ref} and P_e, i.e., $\int_{\delta_0}^{\delta_1}(P_{ref}-P_e)d\delta$, $\int_{\delta_1}^{\delta_u}(P_e-P_{ref})d\delta$, and $\int_{\delta_u}^{\delta_m}(P_{ref}-P_e)d\delta$ are defined as acceleration area A_a, the deceleration area

2168-6777 (c) 2019 IEEE. Personal use is permitted, but republication/redistribution requires IEEE permission. See http://www.ieee.org/publications_standards/publications/rights/index.html for more information.
Authorized licensed use limited to: Aalborg Universitetsbibliotek. Downloaded on March 09,2020 at 13:04:12 UTC from IEEE Xplore. Restrictions apply.

This article has been accepted for publication in a future issue of this journal, but has not been fully edited. Content may change prior to final publication. Citation information: DOI 10.1109/JESTPE.2020.2976791, IEEE Journal of Emerging and Selected Topics in Power Electronics

A_{dmax1} and A_{d2} shown in Fig. 9(b), respectively. Therefore, (13.2) =0 can be rewritten as

$$\int_{\delta_0}^{\delta_1}\left(P_{ref}-P_e\right)d\delta-\int_{\delta_1}^{\delta_u}\left(P_e-P_{ref}\right)d\delta$$
$$-\int_{\delta_u}^{\delta_m}\left(P_{ref}-P_e\right)d\delta=0\Leftrightarrow \quad . \qquad (14)$$
$$A_a-A_{d\max 1}-A_{d2}=0 \quad \text{if } \delta_u\le\delta_m\le\delta_2$$

Define $A_{dma} = \int_{\delta_u}^{\delta_2}(P_{ref}-P_e)d\delta$, as shown in Fig. 9(b). It is apparently that $A_{d2} \le A_{dmax2}$ as $\delta_m \le \delta_2$. Therefore, the sufficient and necessary condition of (14) is given by:

$$A_a-A_{d\max 1}-A_{d\max 2}\le 0 \qquad \text{if } \delta_u\le\delta_m\le\delta_2 . \qquad (15)$$

It is obvious from Fig. 9 (b) that (15) is always true. That ends the proof of 1.3).

It should be noted that A_{dmax2} is the acceleration area for the conventional VSG [21], yet it is changed to the deceleration area by using the mode-adaptive control, which leads to A_a - A_{dmax1}- $A_{dmax2}\le 0$, and thus, the stability of the VSG is enhanced due to the enlarged deceleration area.

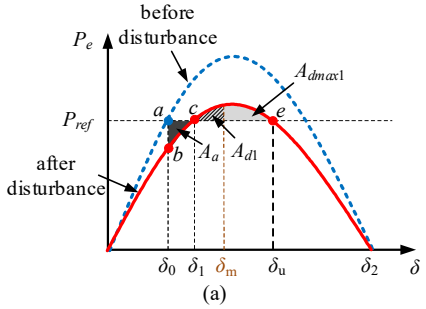

(a)

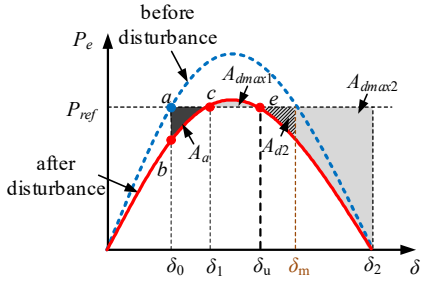

(b)

Fig. 9. Equal area criterion (EAC) for the VSG with the mode-adaptive control. (a) $\delta_1 < \delta_m < \delta_u$. (b) $\delta_u < \delta_m < \delta_2$.

D. Comparison

Table VII compares the transient stability characteristics of the proposed scheme with some existing VSG control methods [7], [9], [23]-[26]. Differing from the conventional VSG control which merely replicates the dynamics of the SG [7], the additional damping correction loop is introduced in [9], which provides another degree of freedom for adjusting the system damping ratio without affecting its steady-state frequency droop characteristic. In [23]-[26], the methods of adaptively changing the inertia and damping ratio of VSGs during large disturbances are proposed to dampen the power and frequency oscillations. While these advanced VSG schemes can improve the transient stability of the system compared to the conventional method, the positive-feedback nature of the power-angle control of the VSG after the UEP is not changed in [9], [23]-[26]. Therefore, transient instability is still inevitable whenever the VSG crosses over the UEP after the transient disturbances.

In contrast, although the mode-adaptive control cannot prevent the VSG from crossing over the UEP either, the loop gain is adaptively switched to change the power angle control from the positive- to negative-feedback dynamics. Thus, the risk of transient instability can be avoided, whenever there are equilibrium points after transient disturbances. This is the unique advantage of the mode-adaptive control compared with prior arts.

IV. Application of the Mode-Adaptive Control in the Power System

Besides the single-VSG-infinite-bus system, the applicability of the proposed mode-adaptive control in the power system with multiple generation units are explored in this section, and the consequent impact on the system-level analysis and protection are also discussed.

TABLE VII
Comparison of the Transient Stability Performance

Post-Disturbance Operations		Conventional VSGs Replicating SG Dynamics [7]	Advanced VSGs with Modified Damping and Inertia Control [9], [23]-[26]	VSG with Mode-Adaptive Control
With equilibrium points		Risk of transient instability	Reduced risk of transient instability	No transient instability
No equilibrium points, without triggering the current limit	Fault cleared FCT < CCT	No transient instability	No transient instability	No transient instability
	Fault cleared FCT> CCT	Unstable	Risk of transient instability	No transient instability
	No fault clearance	Unstable	Unstable	Power angle oscillates around δ_{pk} with the bounded response
No equilibrium points, triggering the current limit		Switch to the current limit control [6], and the transient stability is determined by the current limit and the PLL [13]-[18].		

2168-6777 (c) 2019 IEEE. Personal use is permitted, but republication/redistribution requires IEEE permission. See http://www.ieee.org/publications_standards/publications/rights/index.html for more information.
Authorized licensed use limited to: Aalborg Universitetsbibliotek. Downloaded on March 09,2020 at 13:04:12 UTC from IEEE Xplore. Restrictions apply.

This article has been accepted for publication in a future issue of this journal, but has not been fully edited. Content may change prior to final publication. Citation information: DOI 10.1109/JESTPE.2020.2976791, IEEE Journal of Emerging and Selected Topics in Power Electronics

A. Applicability of Mode-Adaptive Control for Multiple Generators

In the power system with multiple SGs/VSGs, the dynamics of the individual generator, e.g., the *i*th VSG is usually characterized in the center of inertia (COI) reference, in which the power system can be equivalently represented by the virtual COI generator with the system total inertia constant H_T [30]-[31]. Hence, the mode-adaptive control can still be applied to the *i*th VSG provided the virtual COI generator can be treated as the infinite bus during the transient disturbances. This requires the inertia constant of the *i*th mode-adaptive VSG ($H_{i\_adaptive}$) to be much smaller than the system total inertia constant during the disturbance ($H_{T\_disturb}$), i.e., $H_{i\_adaptive} << H_{T\_disturb}$ [31]. It is known from (10) that the mode-adaptive VSG will introduce the negative inertia to the system provided its switching action is triggered during the transient disturbances, which leads to $H_{T\_disturb} \leq H_T$. For the worst case where all mode-adaptive VSGs trigger their switching actions during the disturbance, $H_{i\_adaptive} << H_{T\_disturb}$ can only be met provided $\sum H_{i\_adaptive} << H_T$. Therefore, $\sum H_{i\_adaptive} << H_T$ gives a sufficient (but also conservative) condition for implementing the proposed mode-adaptive control.

On the other hand, when implementing the mode-adaptive control into the power system with multiple SGs/VSGs, $\Delta\omega$ in Fig. 8 should be calculated based on the COI frequency ω_{COI}, i.e., $\Delta\omega=\omega_i-\omega_{COI}$, where ω_{COI} can be obtained from the control center through the communication [32]-[34]. Hence, a fast communication of ω_{COI} is important for applying the mode-adaptive control. In practice, the communication latency can be limited to several milliseconds [35]-[36], which is much faster than the response speed of the power loops of the VSG that dominate its transient stability. Therefore, the proposed method is feasible in practice.

In contrast, the mode-adaptive control cannot be adopted for the VSG that does not satisfy $H_{i\_adaptive} << H_{T\_disturb}$, since the switching action might be wrongly triggered during the swings between multiple SGs/VSGs.

B. Impact of the Proposed Control on the Power System

By using the proposed mode-adaptive control, the transient stability of the individual VSG is enhanced. Yet, the VSG may behave differently from the SG during the fault, which poses new challenges to the power system analysis and protection, which is discussed as follows:

1) Challenge for the system-level transient stability assessment:

The transient stability assessment (TSA) of the SG-dominated power system is mainly based on extensive off-line studies [37], whose credibility is reduced for the modern power system due to the increased penetration of power converters with different control schemes, e.g., the VSG with the proposed mode-adaptive control, as the unpredictable operating conditions of power converters might not be covered in the off-line database. To tackle this challenge, developing the on-line TSA based on the real-time data is needed [37].

2) Challenge for the system-level protection:

2.1. During severe grid faults where the current limit of the VSG is reached, the VSG has to be switched to the vector current control to limit its fault current. In that case, the fault current contributed by the VSG is reduced, which may lead to the malfunction of the overcurrent relay [38].

2.2. During grid faults where the current limit of the VSG is not triggered, the VSG with the proposed mode-adaptive control brings in new challenges to the correct functioning of the out-of-step relay, which is generally designed based on the dynamics of the SG [39].

Overall, the complexities and challenges are due to the fact that the system-level analysis and protection is designed for the SG-dominated power system, whereas the different dynamics introduced by the converter control have not been fully considered. Therefore, the coordination between the converter-level control and the system-level analysis and protection should be carefully re-investigated for the future power electronic based power system.

V. Simulation and Experimental Results

A. Simulation Results

To validate the effectiveness of the proposed method, time-domain simulations are carried out in the MATLAB/Simulink and PLECS blockset with the switching circuit model shown in Fig. 1. The Type-I transient disturbance is considered as the sudden disconnection of the transmission line 2, while the Type-II transient disturbance is considered as the three-phase to ground high-impedance fault on the transmission 2. The parameters given in Table VIII are used. The controller parameters of the VSG are designed based on the guidelines provided in [7]. K_q is chosen as 0.05 pu, which means that the change of 100% output reactive power of the VSG leads to the change of 5% of its output voltage magnitude [7]. The R_g/X_g ratio of the transmission line is chosen as 1/10 [21].

TABLE VIII
Parameters for Transient Disturbance Test (Simulation)

P_{ref}	1000 MW (1 p.u.)	Q_{ref}	0
H	1.65 s	D	0.16 pu
K_q	0.05 p.u.	V_g	220kV/50Hz (1 p.u.)
Test case I		**Test Case II**	
X_T	j0.01 p.u.	X_T	j0.01 p.u.
Z_{g1}	0.10 + j0.95 p.u.	Z_{g1}	0.015 + j0.15 p.u.
Z_{g2}	0.015 + j0.15 p.u.	Z_{g2}	0.08 + j0.8 p.u.
Z_{g3}	j0.01 p.u	Z_{g3}	0.08 + j0.8 p.u.
		Z_{gnd}	0.05 + j0.5 p.u.

1) Type-I transient stability

Fig. 10 shows the simulation results for the Type-I transient stability problem, where the transmission line 2 is disconnected at t=3s. The system parameters of the test case I listed in Table VIII are used. In this case, the system has equilibrium points after the disturbance. Yet, the conventional VSG without adopting the mode-adaptive control (i.e., k =1 always holds) is unstable, as shown in Fig. 10 (a). The oscillation in the output power, power angle and grid currents can be observed, indicating that the VSG loses synchronization with the grid. In contrast, Fig. 10 (b) shows the simulation results of the VSG

2168-6777 (c) 2019 IEEE. Personal use is permitted, but republication/redistribution requires IEEE permission. See http://www.ieee.org/publications_standards/publications/rights/index.html for more information.
Authorized licensed use limited to: Aalborg Universitetsbibliotek. Downloaded on March 09,2020 at 13:04:12 UTC from IEEE Xplore. Restrictions apply.

This article has been accepted for publication in a future issue of this journal, but has not been fully edited. Content may change prior to final publication. Citation information: DOI 10.1109/JESTPE.2020.2976791, IEEE Journal of Emerging and Selected Topics in Power Electronics

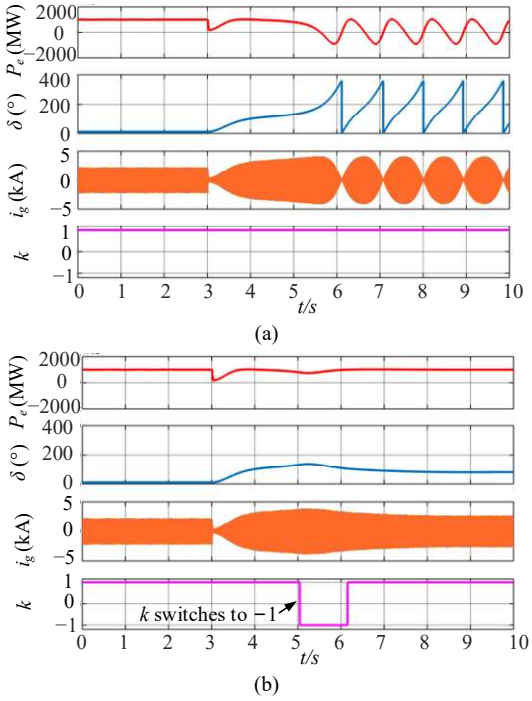

Fig. 10. Simulated dynamic responses of the VSG for the Type-I transient stability problem. (a) Conventional VSG. (b) VSG with the mode-adaptive control.

with the proposed mode-adaptive control. It can be seen that k automatically switches to −1 when the VSG comes into the positive-feedback mode, and switches back to 1 when the VSG moves back to the negative-feedback mode, which guarantees the stable operation of the VSG.

It should be noted that the phase angle δ measured in the simulations and following experiments are merely for illustration purpose, which helps to visualize the stable or unstable operation of the system. The implementation of the mode-adaptive control itself does not require the phase angle information, as shown in Fig. 8.

2) Type-II transient stability

Figs. 11−13 show the simulation results for the symmetrical three-phase to ground, high-impedance fault on the transmission 2. The system parameters of the test case II listed in Table VIII are used. The CCT of the VSG can be calculated in the same way as that of SGs [21], which turns out to be 0.32 s. Three different cases are studied: 1) the fault is not cleared, 2) the fault is cleared with FCT (0.5s) > CCT, and 3) the fault is cleared with FCT (0.2s) < CCT. Since the VSG has no equilibrium points during the fault, the conventional VSG is unstable when the fault is not cleared, as shown in Fig. 11 (a). Yet, with the mode-adaptive control, the VSG does not totally lose the synchronization, as shown in Fig. 11 (b), where k keeps switching between 1 and −1, leading to the power angle oscillates around δ_{pk} in a bounded manner. Moreover, the active power oscillation is also much smaller than that in Fig 11 (a).

In the case that the grid fault is cleared but FCT > CCT, the conventional VSG still becomes unstable, as shown Fig 12 (a), which agrees with the transient stability characteristic of the SG [21]. However, the VSG with the mode-adaptive control becomes stable after the fault is cleared even if FCT > CCT, as shown in Fig. 12 (b). In contrast, both the conventional VSG and the VSG with the mode-adaptive control can be kept stable if FCT < CCT, as shown in Fig 13 (a) and (b).

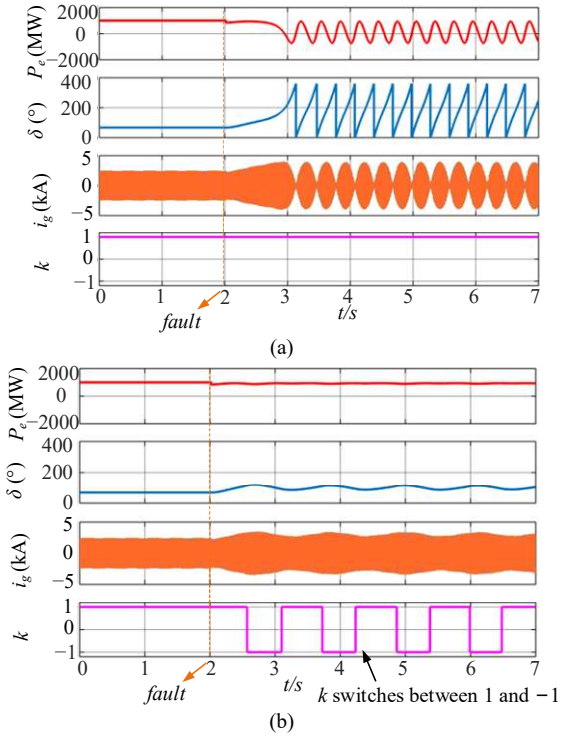

Fig. 11. Simulated dynamic responses of the VSG for the Type-II transient stability problem. The fault is not cleared. (a) Conventional VSG. (b) VSG with the mode-adaptive control.

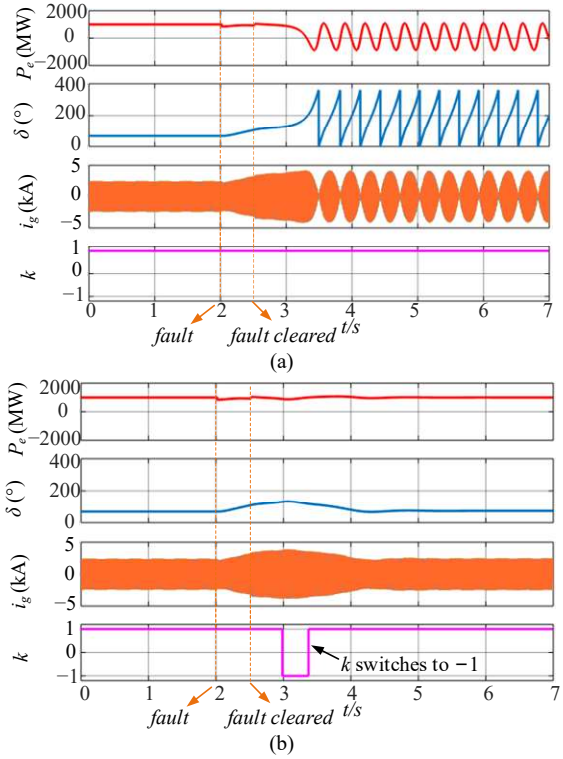

Fig. 12. Simulated dynamic responses of the VSG for the Type-II transient stability problem. The fault is cleared and FCT=0.5s>CCT. (a) Conventional VSG. (b) VSG with the mode-adaptive control.

2168-6777 (c) 2019 IEEE. Personal use is permitted, but republication/redistribution requires IEEE permission. See http://www.ieee.org/publications_standards/publications/rights/index.html for more information.
Authorized licensed use limited to: Aalborg Universitetsbibliotek. Downloaded on March 09,2020 at 13:04:12 UTC from IEEE Xplore. Restrictions apply.

This article has been accepted for publication in a future issue of this journal, but has not been fully edited. Content may change prior to final publication. Citation information: DOI 10.1109/JESTPE.2020.2976791, IEEE Journal of Emerging and Selected Topics in Power Electronics

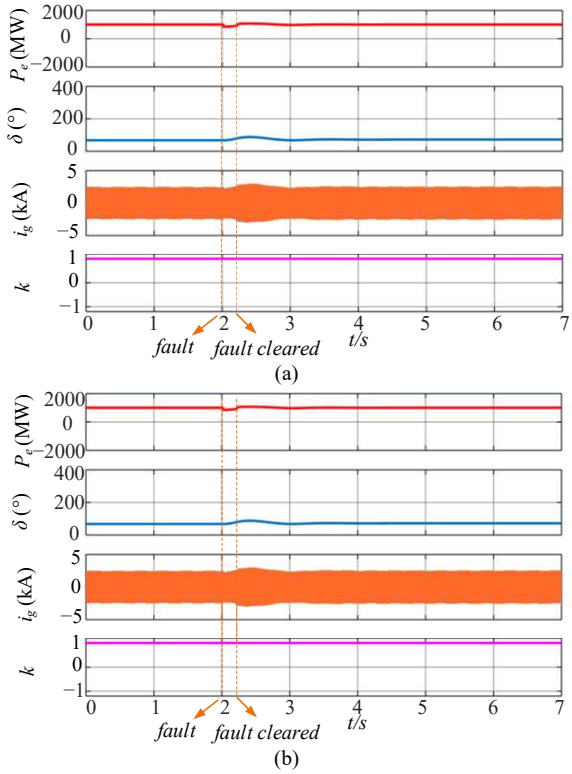

Fig. 13. Simulated dynamic responses of the VSG for the Type-II transient stability problem. The fault is cleared and FCT=0.2s<CCT (a) Conventional VSG. (b) VSG with the mode-adaptive control.

3) Solid fault at the PCC

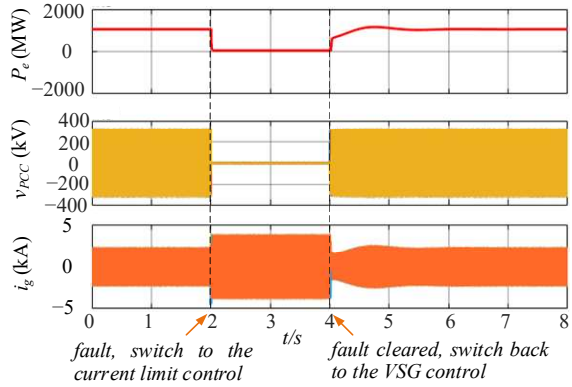

Fig. 14. Simulation results of the VSG with the mode-adaptive control under severe faults at the PCC, the converter switches to the current limit control during the fault and switches back to the mode-adaptive VSG control after the fault clearance.

As mentioned before, the VSG has to be switched to the current control to avoid the overcurrent tripping under the solid fault at the PCC. In that scenario, the grid synchronization is realized by the backup PLL, rather than the active power loop of the VSG [6], and consequently, the mode-adaptive control, which merely modifies the active power loop, has no impact on the dynamics of the current limitation. This fact is confirmed by the simulation results given in Fig. 14. It can be seen that the converter switches to the current limit control during the fault and switches back to the mode-adaptive VSG control after the fault clearance. The current limit is set as 1.8 pu in the simulation. It is clear that the magnitude of the fault current is well controlled within this limit during the fault period.

4) Application of the mode-adaptive control for multiple generators

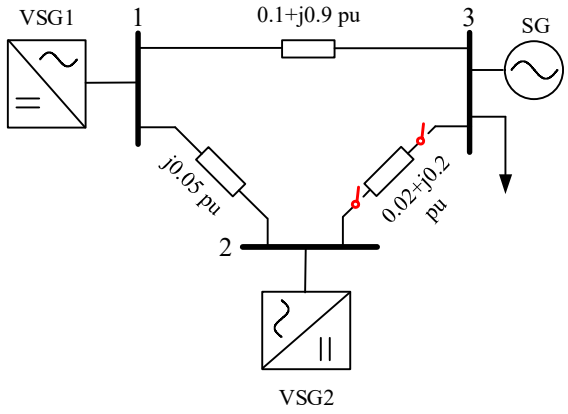

Fig. 15. A 3-bus system with two VSGs and one SG.

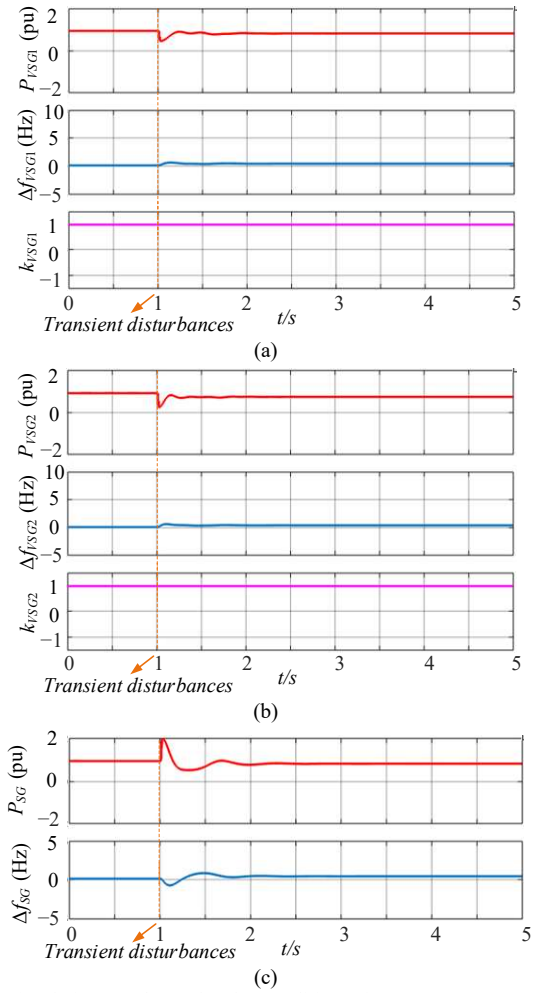

Fig. 16. Simulation results under the condition of H_{VSG1}=1.59s, H_{VSG2}=1.59s, H_{SG}=1.59s, where the mode-adaptive control is not applied to VSG1 and VSG2, and the system is stable. (a) VSG1. (b) VSG2. (c) SG.

To evaluate the applicability of the mode-adaptive control in the power system with multiple generators, case studies on a 3-bus system including two VSGs and one SG are carried out, as

2168-6777 (c) 2019 IEEE. Personal use is permitted, but republication/redistribution requires IEEE permission. See http://www.ieee.org/publications_standards/publications/rights/index.html for more information.
Authorized licensed use limited to: Aalborg Universitetsbibliotek. Downloaded on March 09,2020 at 13:04:12 UTC from IEEE Xplore. Restrictions apply.

This article has been accepted for publication in a future issue of this journal, but has not been fully edited. Content may change prior to final publication. Citation information: DOI 10.1109/JESTPE.2020.2976791, IEEE Journal of Emerging and Selected Topics in Power Electronics

shown in Fig. 15. The transient disturbance is considered as a sudden disconnection of the transmission line between bus 2 and bus 3 at t=1s.

As pointed out in Section IV-A, by using ω_{COI} (a typical 10ms communication delay for obtaining ω_{COI} is considered in the simulation [35]-[36]), the proposed method can be adopted for the ith VSG provided $H_{i\_adaptive}$ << $H_{T\_disturb}$. For verifications, two case studies are carried out:

Case 1: H_{VSG1}=1.59s, H_{VSG2}=1.59s, H_{SG}=1.59s, which leads to H_T = 4.77s. Since even $H_{VSG1,2}$<< H_T is not satisfied, the requirement of $H_{i\_adaptive}$ << $H_{T\_disturb}$ is apparently not met. In this case, the mode-adaptive control cannot work with the VSGs, otherwise unintentional switching actions might be triggered. This is confirmed by the simulation results given in Figs. 16 and 17, where the system is stable after the disturbance if the mode-adaptive control is not used, as shown in Fig. 16, but is destabilized with the mode-adaptive control, as shown in Fig. 17.

Case 2: H_{VSG1}=0.39s, H_{VSG2}=0.39s, H_{SG}=6.4s, which leads to H_T=7.18s. Since H_{VSG1}+ H_{VSG2} << H_T, the criteria $H_{i\_adaptive}$ << $H_{T\_disturb}$ can always be guaranteed. Differing from *Case 1*, the mode-adaptive control can be used with VSGs for enhancing the transient stability of the system. The system becomes unstable after the disturbance when the mode-adaptive control is not used, as shown in Fig. 18, yet it is stabilized after using the mode-adaptive control, as shown in Fig. 19. The simulation results shown in Figs. 16-19 verify the condition ($H_{i\_adaptive}$ << $H_{T\_disturb}$) and the effectiveness of using the mode-adaptive control for enhancing the transient stability of the power system with multiple generators.

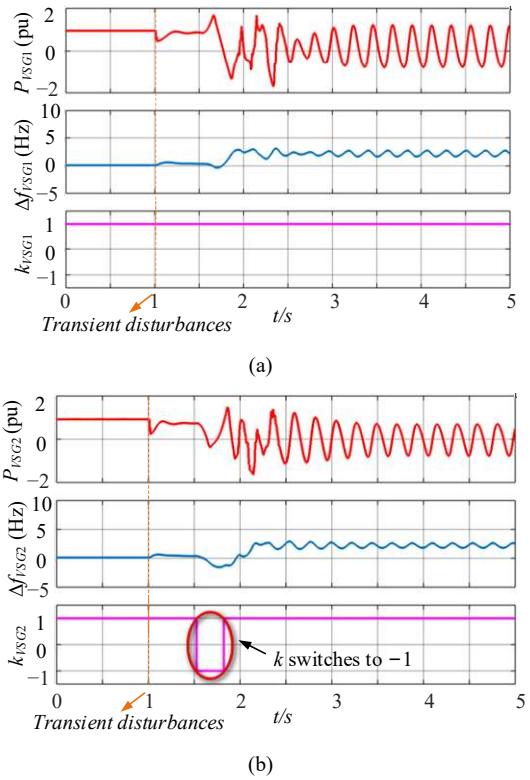

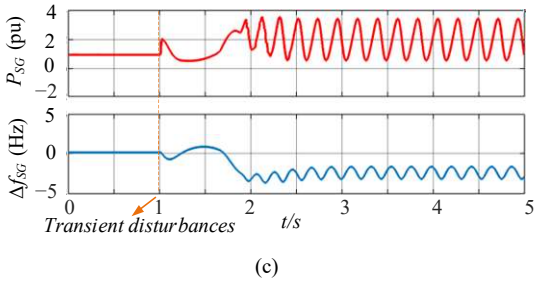

Fig. 17. Simulation results under the condition of H_{VSG1}=1.59s, H_{VSG2}=1.59s, H_{SG}=1.59s, where the mode-adaptive control is applied to VSG1 and VSG2, and the system is unstable. (a) VSG1. (b) VSG2. (c) SG.

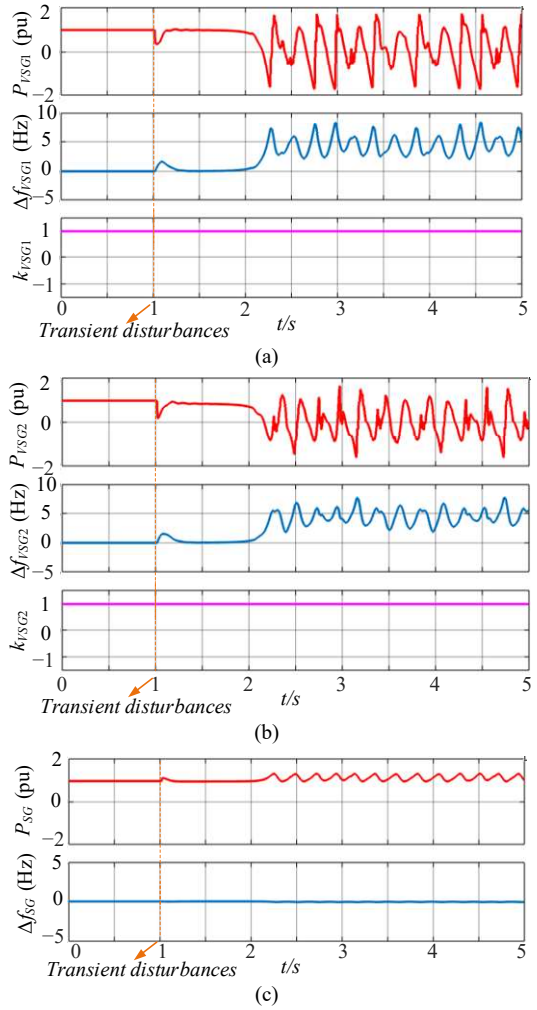

Fig. 18. Simulation results under the condition of H_{VSG1}=0.39s, H_{VSG2}=0.39s, H_{SG}=6.4s, where the mode-adaptive control is not applied to VSG1 and VSG2, and the system is unstable. (a) VSG1. (b) VSG2. (c) SG.

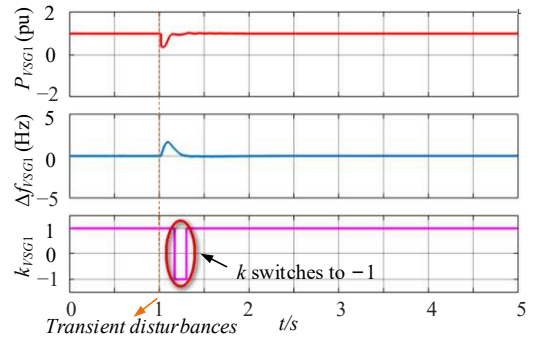

2168-6777 (c) 2019 IEEE. Personal use is permitted, but republication/redistribution requires IEEE permission. See http://www.ieee.org/publications_standards/publications/rights/index.html for more information.
Authorized licensed use limited to: Aalborg Universitetsbibliotek. Downloaded on March 09,2020 at 13:04:12 UTC from IEEE Xplore. Restrictions apply.

This article has been accepted for publication in a future issue of this journal, but has not been fully edited. Content may change prior to final publication. Citation information: DOI 10.1109/JESTPE.2020.2976791, IEEE Journal of Emerging and Selected Topics in Power Electronics

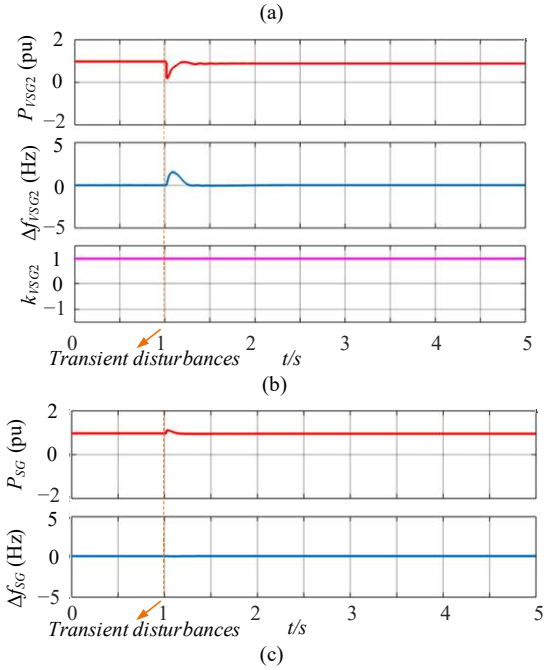

Fig. 19. Simulation results under the condition of H_{VSG1}=0.39s, H_{VSG2}=0.39s, H_{SG}=6.4s, where the mode-adaptive control is applied to VSG1 and VSG2, and the system is stable. (a) VSG1. (b) VSG2. (c) SG.

B. Experimental Results

To further verify the simulation results, the experiments are carried out with a three-phase grid-connected converter with downscaled voltage and power ratings. Yet, the per unit values of parameters used in the experiment are same as that used in simulations, which are summarized in Table IX. The same transient disturbances considered in simulations are evaluated in experiments.

Fig. 20 shows the layout of the experimental setup. The control algorithm is implemented in the DS1007 dSPACE system, where the DS2004 high-speed A/D board is used for the voltage and current measurements. The DS2102 high-speed D/A board is used to transmit the calculated active power, power angle and the gain k, to the oscilloscope. In addition, a constant dc voltage supply is used at the dc-side, and a 45 kVA Chroma 61850 grid simulator is used to emulate the infinite bus.

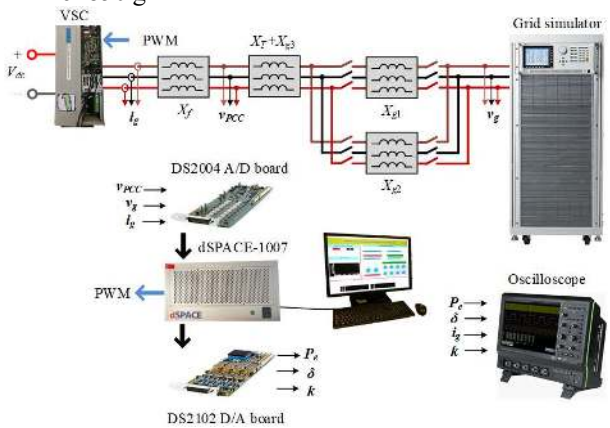

Fig. 20. Configuration of the experimental setup.

TABLE IX
PARAMETERS FOR TRANSIENT DISTURBANCE TEST (EXPERIMENTS)

P_{ref}	1 kW (1 p.u.)	Q_{ref}	0
H	1.65 s	D	0.16 pu
K_q	0.05 p.u.	V_g	50V/50Hz (1 p.u.)
Test case I		**Test Case II**	
X_T	j0.01 p.u.	X_T	j0.01 p.u.
Z_{g1}	0.10 + j0.95 p.u.	Z_{g1}	0.015 + j0.15 p.u.
Z_{g2}	0.015 + j0.15 p.u.	Z_{g2}	0.08 + j0.8 p.u.
Z_{g3}	j0.01 p.u	Z_{g3}	0.08 + j0.8 p.u.
		Z_{gnd}	0.05 + j0.5 p.u.

Fig. 21 provides the experimental results for the Type-I transient stability case, i.e., the sudden disconnection of the transmission line 2. The parameters of the test case I listed in Table IX are used, and the system has equilibrium points after the disturbance. It can be seen that the conventional VSG becomes unstable in this scenario, as shown in Fig. 21(a), which agrees with the simulation results in Fig. 10(a). In contrast, the VSG with the mode-adaptive control scheme can still be kept stable, as shown in Fig. 21(b), which confirms the simulation result in Fig. 10(b). As the background noise is inevitable in practice, the low-pass filter (LPF) is added after calculating d(ΔP)/dt in the experiment, which leads to the slightly slower dynamic of switching the gain compared with simulation results. Nevertheless, the LPF will not affect the effectiveness of the control method for the transient stability enhancement, which is supported by the experimental results given in Figs. 21-24.

Figs. 22-24 show the experimental results of the symmetrical three-phase to ground high impedance fault on the transmission line 2. The parameters of the test case II listed in Table IX are used, and the system does not have equilibrium points during the fault. The CCT of the VSG is calculated as 0.32 s. Following the simulation studies, three different cases are tested: 1) the fault is not cleared, 2) the fault is cleared with FCT (0.5s) > CCT, and 3) the fault is cleared with the FCT (0.2s) < CCT.

From Figs. 22(a) and 23(a), it is clear that the conventional VSG loses synchronism with the power grid when the fault is not cleared or when the fault is cleared with FCT > CCT. Yet, with the mode-adaptive control scheme, the power angle of the VSG is still bounded even if the fault is not cleared, as shown in Fig. 22(b), and the system can be kept stable even if the fault is cleared with FCT > CCT, as shown in Fig. 23(b). These tests confirm again the effectiveness of the proposed method.

Fig. 24 shows the measured results for both the conventional VSG and the VSG with the mode-adaptive control scheme in the case that the fault is cleared with FCT < CCT. It can be seen that the system can be kept stable in both cases. This also corroborates the effectiveness of the calculated CCT.

2168-6777 (c) 2019 IEEE. Personal use is permitted, but republication/redistribution requires IEEE permission. See http://www.ieee.org/publications_standards/publications/rights/index.html for more information.
Authorized licensed use limited to: Aalborg Universitetsbibliotek. Downloaded on March 09,2020 at 13:04:12 UTC from IEEE Xplore. Restrictions apply.

This article has been accepted for publication in a future issue of this journal, but has not been fully edited. Content may change prior to final publication. Citation information: DOI 10.1109/JESTPE.2020.2976791, IEEE Journal of Emerging and Selected Topics in Power Electronics

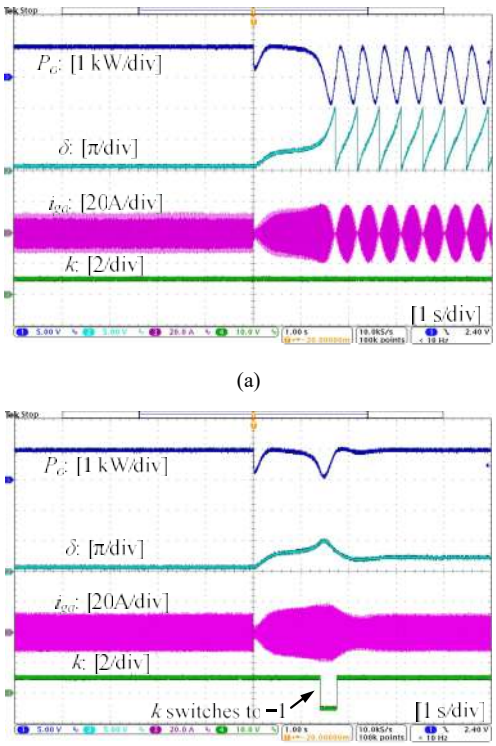

Fig. 21. Experimental results of the VSG for the Type-I transient stability problem. (a) Conventional VSG. (b) VSG with the mode-adaptive control.

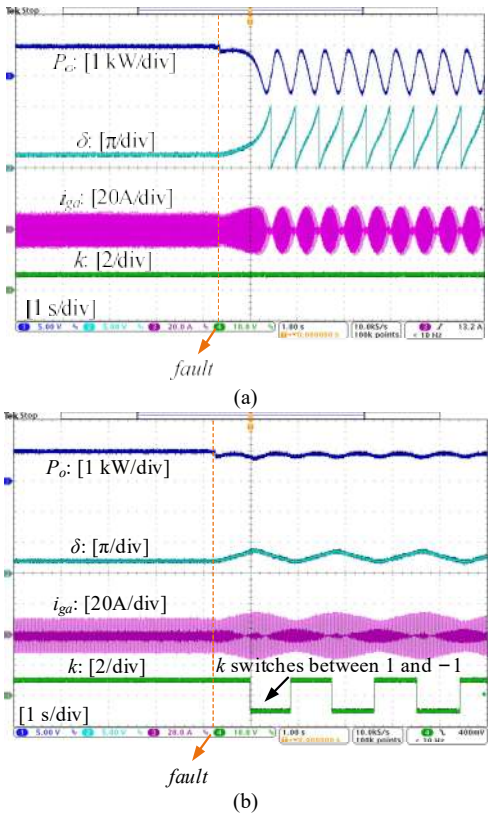

Fig. 22. Experimental results of the VSG for the Type-II transient stability problem. The fault is not cleared. (a) Conventional VSG. (b) VSG with the mode-adaptive control.

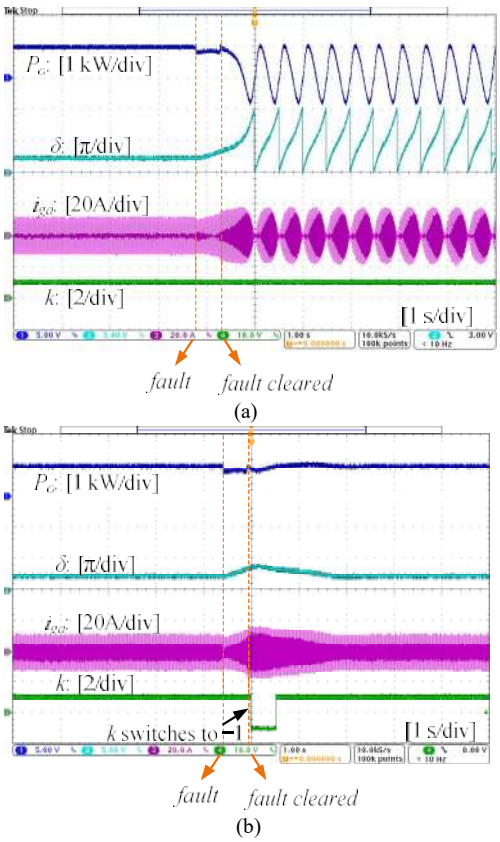

Fig. 23. Experimental results of the VSG for the Type-II transient stability problem. The fault is cleared and FCT=0.5s>CCT. (a) Conventional VSG. (b) VSG with the mode-adaptive control.

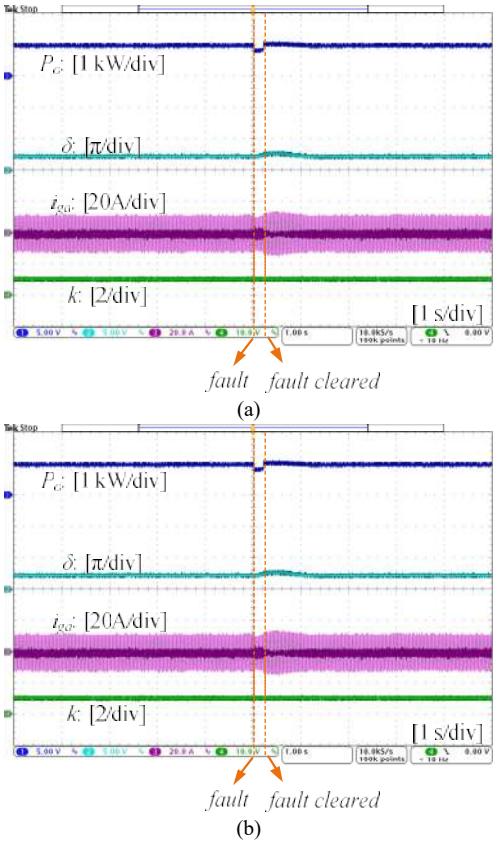

2168-6777 (c) 2019 IEEE. Personal use is permitted, but republication/redistribution requires IEEE permission. See http://www.ieee.org/publications_standards/publications/rights/index.html for more information.
Authorized licensed use limited to: Aalborg Universitetsbibliotek. Downloaded on March 09,2020 at 13:04:12 UTC from IEEE Xplore. Restrictions apply.

This article has been accepted for publication in a future issue of this journal, but has not been fully edited. Content may change prior to final publication. Citation information: DOI 10.1109/JESTPE.2020.2976791, IEEE Journal of Emerging and Selected Topics in Power Electronics

Fig. 24. Experimental results of the VSG for the Type-II transient stability problem. The fault is cleared and FCT=0.2s<CCT (a) Conventional VSG. (b) VSG with the mode-adaptive control.

VI. Conclusion

This paper proposes a simple yet effective approach for enhancing the transient stability of the VSG. Simulations and experimental case studies have been presented. The transient stability problems for the VSGs with and without equilibrium points after the disturbance have been considered. The proposed method can be adopted for the VSG in the power system when $H_{i\_adaptive} << H_{T\_disturb}$, and it yields a superior performance compared with the conventional VSG control method. A competitive advantage of the mode-adaptive control scheme is the VSG can be kept stable even if the fault is cleared beyond the CCT derived based on the conventional SG-based systems.

References

[1] F. Blaabjerg, R. Teodorescu, M. Liserre, and A. V. Timbus, "Overview of control and grid synchronization for distributed power generation systems," *IEEE Trans. Ind. Electron.*, vol. 53, no. 5, pp. 1398–1409, Oct. 2006.

[2] X. Wang and F. Blaabjerg, "Harmonic stability in power electronic based power systems: concept, modeling, and analysis," *IEEE Trans. Smart Grid*., vol. 10, no. 3, pp. 2858–2870, May. 2019.

[3] H.-P. Beck and R. Hesse, "Virtual synchronous machine," in *Proc. 9th Int. Conf. Elect. Power Qual. Util. (EPQU)*, 2007, pp. 1–6.

[4] Q. C. Zhong and G. Weiss, "Synchronverters: Inverters that mimic synchronous generators," *IEEE Trans. Ind. Electron.*, vol. 58, no. 4, pp. 1259–1267, Apr. 2011.

[5] J. Fang, H. Li, Y. Tang and F. Blaabjerg, "On the inertia of future more-electronics power systems," *IEEE J. Emerg. Sel. Topics Power Electron.*, early access, pp. 1–1, 2018.

[6] L. Zhang, L. Harnefors, and H. –P. Nee. "Power-synchronization control of grid-connected voltage-source converters". *IEEE Trans. Power Syst.,* vol. 25, no. 2, pp. 809−820, May. 2010.

[7] H. Wu, X. Ruan, D. Yang, X. Chen, W. Zhao, Z. Lv and Q. C. Zhong, "Small-signal modeling and parameters design for virtual synchronous generators," *IEEE Trans. Ind. Electron.*, vol. 64, no. 7, pp. 4292–4303, Jul. 2016.

[8] J. Fang, Y. Tang, H. Li, and X. Li, "A battery/ultracapacitor hybrid energy storage system for implementing the power management of virtual synchronous generators," *IEEE Trans. Power Electron.,* vol. 33, no. 4, pp. 2820-2824, Apr. 2018.

[9] S. Dong and Y. C. Chen, "Adjusting synchronverter dynamic response speed via damping correction loop," *IEEE Trans. Energy Convers*., vol. 32, no. 2, pp. 608–619, Jun. 2017.

[10] Z. Shuai, C. Shen, X. Liu, Z. Li and Z. J. Shen, "Transient angle stability of virtual synchronous generators using Lyapunov's direct method, " *IEEE Trans. Smart Grid.*, early access, pp. 1–1, 2018.

[11] H. Wu and X. Wang, "Design-oriented transient stability analysis of grid-connected converters with power synchronization control" *IEEE Trans. Ind. Electron.*, vol. 66, no. 8, pp. 6473–6482, Aug. 2019.

[12] D. Pan, X. Wang, F. Liu and R. Shi, "Transient stability of voltage-source converters with grid-forming control: a design-oriented study," *IEEE J. Emerg. Sel. Topics Power Electron.*, early access, pp. 1–1, 2019.

[13] L. Huang, H. Xin, Z. Wang, L. Zhang, K. Wu, and J. Hu, "Transient stability analysis and control design of droop-controlled voltage source converters considering current limitation," *IEEE Trans. Smart Grid*, vol. 10, no. 1, pp. 578-591, Jan. 2019.

[14] H. Geng, L. Liu, and R. Li, "Synchronization and reactive current support of PMSG based wind farm during severe grid fault," *IEEE Trans. Sustain. Energy*, vol. PP, no. 99, pp. 1–1, 2018.

[15] D. Dong, B. Wen, D. Boroyevich, P. Mattavelli, and Y. Xue, "Analysis of phase-locked loop low-frequency stability in three-phase grid-connected power converters considering impedance interactions," *IEEE Trans. Ind. Electron*., vol. 62, no. 1, pp. 310–321, Jan. 2015.

[16] O. Göksu, R. Teodorescu, C. L. Bak, F. Iov, and P. C. Kjær, "Instability of wind turbine converters during current injection to low voltage grid faults and PLL frequency based stability solution," *IEEE Trans. Power Syst.,* vol. 29, no.4, pp. 1683–1691, July 2014.

[17] H. Wu and X. Wang, "Design-oriented transient stability analysis of PLL-synchronized voltage-source converters," *IEEE Trans. Power Electron.*, vol. 35, no. 4, pp. 3573-3589, Apr. 2020.

[18] M. Taul, X. Wang, P. Davari and F. Blaabjerg, "An overview of assessment methods for synchronization stability of grid-connected converters under severe symmetrical grid faults," *IEEE Trans. Power Electron.*, vol. 34, no. 10, pp. 9655-9670, Oct. 2019.

[19] D. C. T. Wai and X. Yibin, "A novel technique for high impedance fault identification," *IEEE Trans. Power Del.,* vol. 13, no. 3, pp. 738–744, July 1998.

[20] National Grid ESO, "Performance of phase-locked loop based converters," Warwick, UK, 2017, [Online]. Available: https://www.nationalgrideso.com/insights/system-operability-framework-sof

[21] P. Kundur, *Power System Stability and Control*. New York, NY, USA: McGraw-Hill, 1994.

[22] AIEE Committee Report, "First report of power system stability", *AIEE Transactions*, Vol. 56, Feb. 1937, pp. 261-282.

[23] J. Alipoor, Y. Miura, and T. Ise, "Power system stabilization using virtual synchronous generator with alternating moment of inertia," *IEEE J. Emerg. Sel. Topics Power Electron.*, vol. 3, no. 2, pp. 451–458, Jun. 2015.

[24] D. Li, Q. Zhu, S. Lin, and X. Y. Bian, "A self-adaptive inertia and damping combination control of VSG to support frequency stability," *IEEE Trans. Energy Conv.,* vol. 32, no. 1, pp. 397-398, Mar. 2017.

[25] M. A. Torres L, L. A. C. Lopes, L. A. Moran T, and J. R. Espinoza C., "Self-tuning virtual synchronous machine: a control strategy for energy storage systems to support dynamic frequency control," *IEEE Trans. Energy Convers.*, vol. 29, no. 4, pp. 833–840, Dec. 2014.

[26] X. Hou, H. Han, C. Zhong, W. Yuan, M. Yi, and Y. Chen, "Improvement of transient stability in inverter-based ac microgrid via adaptive virtual inertia," in *2016 IEEE Energy Conversion Congress and Exposition (ECCE)*, Sept 2016, pp. 1–6.

[27] Y. W. Li and C.-N. Kao, "An accurate power control strategy for power electronics-interfaced distributed generation units operating in a low voltage multi bus microgrid," *IEEE Trans. Power Electron.*, vol. 24, no.12, pp. 2977-2988, Dec. 2009.

[28] L. Harnefors, X. Wang, A. Yepes, and F. Blaabjerg, "Passivity-based stability assessment of grid-connected VSCs - an overview," *IEEE Jour. Emer. Select. Top. Power Electron.*, vol. 4, no. 1, pp. 116-125, Mar. 2016.

[29] J.-J. E. Slotine and W. Li, *Applied Nonlinear Control*. Englewood Cliffs, NJ: Prentice-Hall, 1991.

[30] A. Michel, A. Fouad, and V. Vittal, "Power system transient stability using individual machine energy functions," *IEEE Trans. Circuits Syst*., vol. 30, no. 5, pp. 266–276, 1983.

[31] S. Wang, J. Yu, and W. Zhang, ''Transient stability assessment using individual machine equal area criterion PART I: Unity principle,'' *IEEE Access*, vol. 6, pp. 77065–77076, 2018.

[32] S. E. Stanton, C. Slivinsky, K. Martin, and J. Nordstrom, "Application of phasor measurements and partial energy analysis in stabilizing large disturbances," *IEEE Trans. on Power Systems*, vol. PWRS-10, no. 1, pp. 297–306, Feb. 1995.

[33] F. Milano, "Rotor speed-free estimation of the frequency of the center of inertia," *IEEE Trans. Power Syst.,* vol. 33, no. 1, pp. 1153–1155, Jan. 2018.

[34] J. B. Zhao, Y. Tang, and V. Terzija, "Robust online estimation of power system center of inertia frequency," *IEEE Trans. Power Syst.*, vol. 34, no. 1, pp. 821–825, Jan. 2019.

[35] X. Xie, W. Liu, H. Liu, Y. Du, and Y. Li, "A system-wide protection against unstable SSCI in series-compensated wind power systems," *IEEE Trans. Power Del.* vol. 33, no. 6, pp. 3095–3104, Dec. 2018.

[36] L. Cheng, G. Chen, W. Gao, F. Zhang, and G. Li, "Adaptive time delay compensator (ATDC) design for wide-area power system stabilizer," *IEEE Trans. Smart Grid*, vol. 5, no. 6, pp. 2957–2966, Nov. 2014.

[37] J. Weckesser, "On-line dynamic security assessment in power systems". *Ph.D. dissertation*, Department of Electrical Engineering. Technical University of Denmark, 2014.

[38] A. Abdalrahman and E. Isabegovic, "DolWin1 - Challenges of connecting offshore wind farms," *in Proc. 2016 IEEE Int. Energy Conf*., Apr. 2016, pp. 1–10.

2168-6777 (c) 2019 IEEE. Personal use is permitted, but republication/redistribution requires IEEE permission. See http://www.ieee.org/publications_standards/publications/rights/index.html for more information.
Authorized licensed use limited to: Aalborg Universitetsbibliotek. Downloaded on March 09,2020 at 13:04:12 UTC from IEEE Xplore. Restrictions apply.

This article has been accepted for publication in a future issue of this journal, but has not been fully edited. Content may change prior to final publication. Citation information: DOI 10.1109/JESTPE.2020.2976791, IEEE Journal of Emerging and Selected Topics in Power Electronics

[39] D. Tziouvaras and D. Dou, Out-of-Step protection fundamentals and advancements [Online]. Available: http://www.selinc.com/techpprs/6163.pdf.

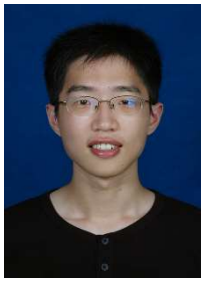

Heng Wu (S'17) received the B.S. and M.S. degrees in electrical engineering from Nanjing University of Aeronautics and Astronautics (NUAA), Nanjing, China, in 2012 and 2015, respectively. He is currently working toward the Ph.D. degree in power electronic engineering in Aalborg University, Aalborg, Denmark.

From 2015 to 2017, He was an Electrical Engineer with NR Electric Co., Ltd, Nanjing, China. He was a guest researcher with Ørsted Wind Power, Fredericia, Denmark, from November to December, 2018, and with Bundeswehr University Munich, Germany, from September to December, 2019. His research interests include the modelling and stability analysis of the power electronic based power systems.

Xiongfei Wang (S'10-M'13-SM'17) received the B.S. degree from Yanshan University, Qinhuangdao, China, in 2006, the M.S. degree from Harbin Institute of Technology, Harbin, China, in 2008, both in electrical engineering, and the Ph.D. degree in energy technology from Aalborg University, Aalborg, Denmark, in 2013.

Since 2009, he has been with the Department of Energy Technology, Aalborg University, where he became an Assistant Professor in 2014, an Associate Professor in 2016, a Professor and Research Program Leader for Electronic Power Grid (eGrid) in 2018, and the Director of Aalborg University-Huawei Energy Innovation Center in 2020. His current research interests include modeling and control of grid-interactive power converters, stability and power quality of converter-based power systems, active and passive filters.

Dr. Wang was selected into Aalborg University Strategic Talent Management Program in 2016. He has received six IEEE Prize Paper Awards, the 2016 Outstanding Reviewer Award of IEEE Transactions on Power Electronics, the 2018 IEEE PELS Richard M. Bass Outstanding Young Power Electronics Engineer Award, the 2019 IEEE PELS Sustainable Energy Systems Technical Achievement Award, and the 2019 Highly Cited Researcher by Clarivate Analytics (former Thomson Reuters). He serves as a Member at Large for Administrative Committee of IEEE Power Electronics Society in 2020-2022, and as an Associate Editor for the IEEE Transactions on Power Electronics, the IEEE Transactions on Industry Applications, and the IEEE Journal of Emerging and Selected Topics in Power Electronics.

2168-6777 (c) 2019 IEEE. Personal use is permitted, but republication/redistribution requires IEEE permission. See http://www.ieee.org/publications_standards/publications/rights/index.html for more information.
Authorized licensed use limited to: Aalborg Universitetsbibliotek. Downloaded on March 09,2020 at 13:04:12 UTC from IEEE Xplore. Restrictions apply.